

Circularly Polarized Near-field Scanning Optical Microscope for Investigations of Edge States of a Two-dimensional Electron System

Shintaro Nomura · Syuhei Mamyouda · Hironori Ito · Yusuke Shibata ·
Tomoya Ohira · Luno Yoshikawa · Youiti Ootuka · Satoshi Kashiwaya ·
Masumi Yamaguchi · Hiroyuki Tamura · Tatsushi Akazaki

Received: date / Accepted: date

Abstract We report on investigations of the quantum-Hall chiral edge states using a near-field scanning optical microscope that enables us to irradiate circularly polarized light from the probe tip with spatial resolution below the diffraction limit. We have found a clear evidence for the formation of spin-split incompressible strips near the edge of a two-dimensional electron system in high magnetic fields.

Keywords near-field scanning optical microscope · quantum Hall effect · spin injection

1 Introduction

A near-field scanning optical microscope (NSOM) [1, 2] has been intensively utilized to investigate optical properties of semiconductors at spatial resolution below the diffraction limit. NSOMs have been successfully providing a method to clarify phenomena closely related to charge distributions and the potential profiles in semiconductors such as ground- and excited-states in single self-assembled quantum dots [3], localization

This work was partly supported by Kakenhi Nos. 25103704, 26610079, 15H03673.

S. Nomura · S. Mamyouda · H. Ito · Y. Shibata · T. Ohira ·
L. Yoshikawa · Y. Ootuka
Division of Physics, Univ. of Tsukuba, 1-1-1 Tennoudai,
Tsukuba 305-8571, Japan
Fax: +81-29-8536618
E-mail: nomura.shintaro.ge@u.tsukuba.ac.jp

S. Kashiwaya
National Institute of Advanced Industrial Science and
Technology, 1-1-1 Umezono, Tsukuba, 305-8568, Japan

M. Yamaguchi · H. Tamura · T. Akazaki
NTT Basic Research Laboratories, 3-1 Morinosato-
Wakamiya, Atsugi, 243-0198, Japan

of the electrons in the random potential [4], imaging of excitons and biexcitons in naturally occurring quantum dots [5], and the edge of a two-dimensional electron system (2DES) in high magnetic field [6]. By contrast, applications of NSOMs to investigate spin properties of semiconductors have been very limited, mainly because of the difficulty in emitting or detecting circularly polarized light using an NSOM probe tip since the polarization is disturbed by birefringence induced by small tensions or torsions at the NSOM probe tip. Here we report on our successful development of circularly polarized NSOM and investigations of the spin-dependent properties of the edge states of a 2DES [7].

2 Methods

2.1 Experimental

We used a method to control the polarization of the light emitted from an NSOM probe by controlling the polarization of the incident light with a Berek compensator [7]. A double tapered NSOM probe was prepared by the method described in the literatures [8, 7]. We have fabricated an NSOM probe tip with an aperture with good axial symmetry by focused ion beam slicing of the apex of the probe tip. Furthermore, cares have been taken to avoid any stress or torsion by twisting or bending to minimize possible extrinsic birefringence in high magnetic field region using a dilution refrigerator specially designed for this purpose. This minimizes possible birefringence accompanied by the Faraday effect for a diamagnetic material [9]. The compensation parameter of the Berek compensator is mostly explained by the extrinsic birefringence added by a single turn coil of the optical fiber with radius (r) of 0.25 m that

is located outside of the cryostat and is mechanically supported by an aluminum rail as shown in Fig. 1 in order to fix the path of the optical fiber.

We used a Hall-bar structure of a GaAs/Al_{0.3}Ga_{0.7}As single heterojunction with the mobility and the electron density of 180 m²/Vs and 4.6×10^{11} cm⁻², respectively. The optical excitation power was 1.1 nW at the excitation photon energy of 1.5140 eV, which is 5.7 meV above the onset of the absorption of GaAs single heterojunction. Measurements were performed using a tube piezoscanner and a piezoelectric inertial sliding stage at 250 mK in magnetic fields perpendicular to the sample surface in a dilution refrigerator. Photovoltage between the ohmic contacts 1 and 2 in Fig. 1 was detected synchronously with a lock-in amplifier at 159 Hz.

2.2 Theory

The electronic structure of spin-resolved states near the sample edge in perpendicular magnetic field B is calculated based on the local-spin-density approximation formalism [7, 10, 11]. The Hamiltonian is given by

$$H = H_0 + V_c(\mathbf{r}) + V_H(n, \mathbf{r}) + V_x^s(n^\uparrow, n^\downarrow, \mathbf{r}) + \frac{g_c \mu_B}{\hbar} s_z B \quad (1)$$

where

$$H_0 = -\frac{\hbar^2}{2m^*} \left[\frac{\partial^2}{\partial x^2} + \frac{\partial^2}{\partial z^2} - \left(\frac{1}{i} \frac{\partial}{\partial y} + \frac{eBx}{\hbar} \right)^2 \right] \quad (2)$$

is the kinetic energy in the Landau gauge $\mathbf{A} = (0, Bx, 0)$ and V_c , V_H , and V_x^s are the confinement potential, the Hartree term, and the exchange-energy term, $n^s(\mathbf{r})$ is the electron charge density for spin $s = \uparrow, \downarrow$ at finite temperature, and g_c , μ_B , and m^* are the effective electron g -factor, the Bohr magneton, and the electron effective mass. A plane-wave basis set is used for the y -direction. The center of the cyclotron-motion X is given by $X = -l_B^2 k_y$, where l_B and k_y are the magnetic length and the wavevector in the y -direction. The higher-order finite difference method [10, 12] is used in two-dimensional grids of 690×7 and 690×33 per unit cell for the calculations of the wave function and the potential, respectively, for the x - and z directions. The confinement potential is given by $V_c(\mathbf{r}) = V_l(x) + V_z(z)$. We consider a quantum wire structure with a width of 3150 nm, assuming lateral confinement potentials of $V_l(x) = V_0(x) + V_4(x)$, and $V_l(x) = V_0(x) + V_2(x)$. We assume $V_0 = 1000$ eV for $x < 0$ and $x > 3150$ nm and 0 eV for $0 \leq x \leq 3150$ nm, and consider $V_4(x) = C_4(x - x_0)^4$, and $V_2(x) = \frac{m}{2} \omega_0^2 (x - x_0)^2$ as shown in Fig. 2, where we use $x_0 = 2500$ nm, $C_4 = 8.37 \times 10^{-15}$

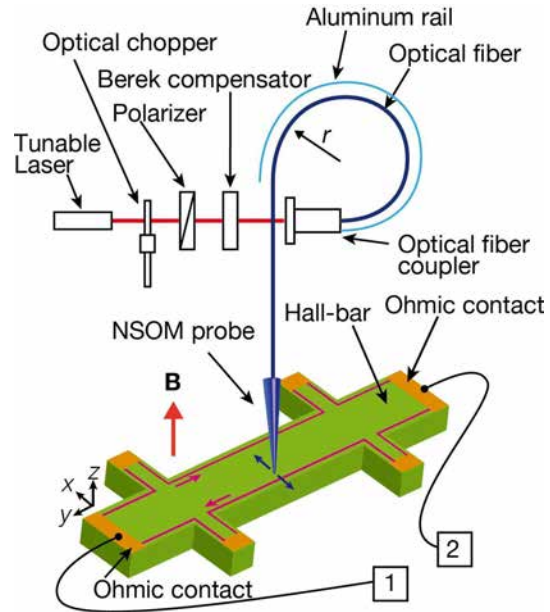


Fig. 1 Schematics of measurement setup. The photo voltage between the ohmic contacts 1 and 2 is measured by scanning the position of the NSOM probe on the surface of a Hall-bar structure. Magnetic field is applied perpendicular to the surface of the sample.

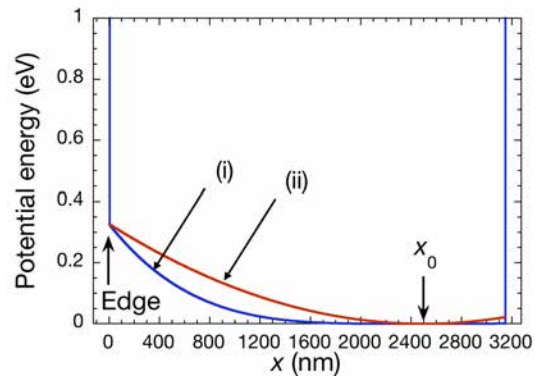


Fig. 2 Lateral confinement potentials assumed in the calculations, (i) fourth-order polynomial and (ii) parabolic confinement potentials.

eV/nm⁴, and $\hbar\omega_0 = 0.3465$ meV that give the depletion layer thickness of 134 nm and determine the size of the edge states. For the vertical confinement potential, we set $V_z(z) = 0$ eV for $90 \leq z \leq 115$ nm and 0.270 eV elsewhere. Material parameters for GaAs and AlAs can be found in the literatures [13]. Details of the calculation can be found elsewhere [7]

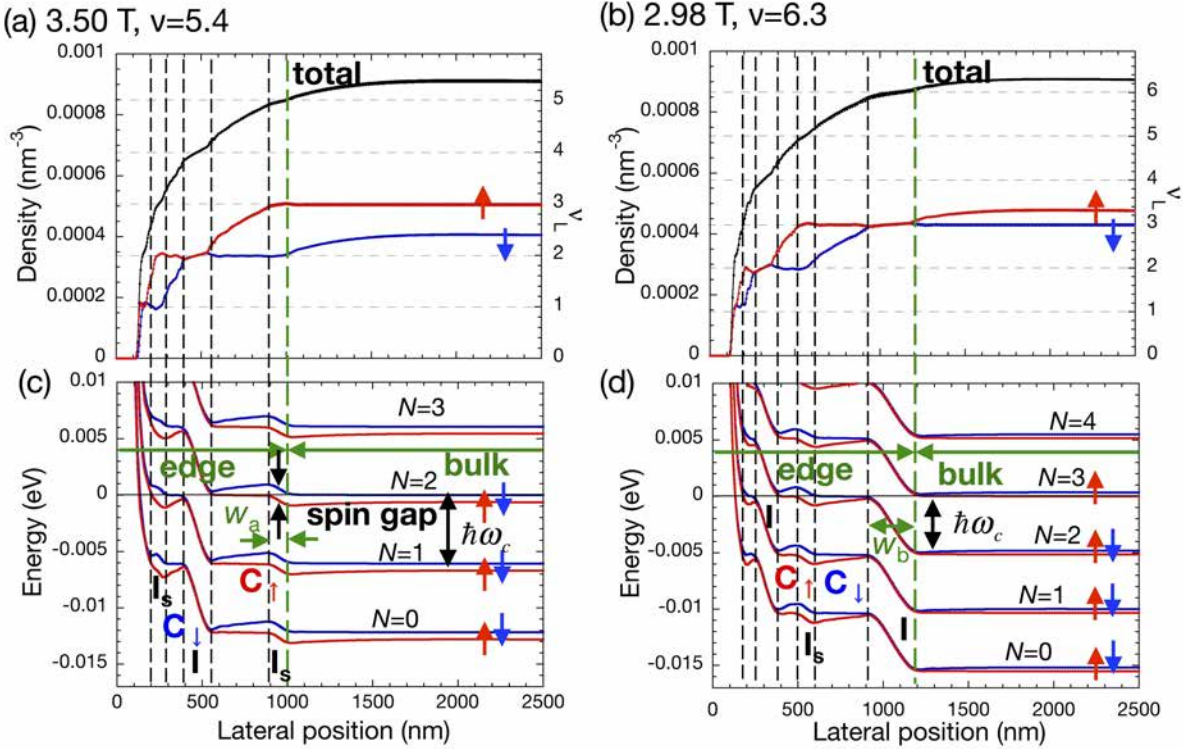


Fig. 3 Calculated electron densities near the sample edge for (a) $\nu = 5.4$ and (b) $\nu = 6.3$, by using $V_4(x)$. The black curve denotes the total density and the red and blue curves denote the densities for up- and down-spin electrons, respectively, as functions of x . ν_L denotes the local electron filling factor. Calculated subband structures for (c) $\nu = 5.4$ and (d) $\nu = 6.3$ as functions of the center of the cyclotron motion X . The red and blue curves denote the subbands for up- and down-spin electrons, respectively. w_a and w_b denote the widths of the innermost incompressible strips. N denotes the Landau level index. The origin of the energy is taken at the Fermi level.

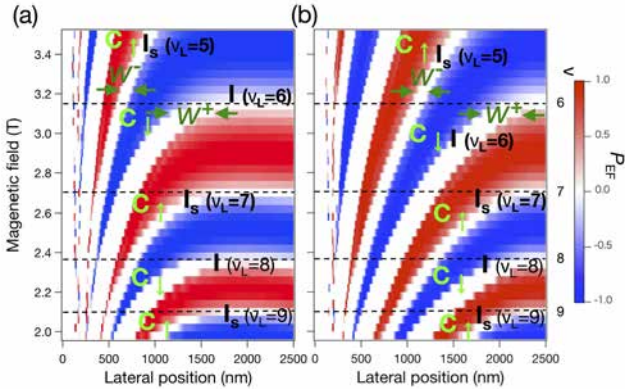


Fig. 4 Calculated occupations near the Fermi level as defined by Eq. (3) for (a) fourth-order polynomial and (b) parabolic confinement potentials as functions of X . w^+ and w^- denote the widths of the innermost incompressible strips at ν^+ and ν^- , respectively.

3 Results and Discussions

3.1 Compressible and incompressible strips

The alternating strips of the compressible and incompressible liquids are formed near the edge of the 2DES

in a magnetic field due to the screening of the confinement potential [14–17,10,18] as shown in Fig. 3, calculated by using $V_4(x)$. There is a region of constant electron density with a finite energy gap at the Fermi level. The spin-unpolarized incompressible strip (I) is formed in the case where the energy gap is opened due to the cyclotron energy $\hbar\omega_c$, and the spin-split incompressible strip (I_s) is formed due to the exchange energy-enhanced spin gap [19] in high magnetic fields as shown in Fig. 3. In-between the spin-unpolarized and spin-split incompressible strips, there are regions of smoothly varying electron density and of constant subband energy of either up- or down-spin electrons, called the spin-polarized compressible strips (C_\uparrow , C_\downarrow).

Figure 4 shows calculated occupations near the Fermi level for $V_4(x)$ and $V_2(x)$ as defined by

$$P_{E_F} = \frac{1}{f'(E_F)} \left[\sum_j f'(E_{j,k_y,\uparrow}(B)) - f'(E_{j,k_y,\downarrow}(B)) \right] \quad (3)$$

where $f'(E)$ is the first derivative of the Fermi distribution function at $T = 0.25$ K, and $E_{j,k_y,s}(B)$ is the

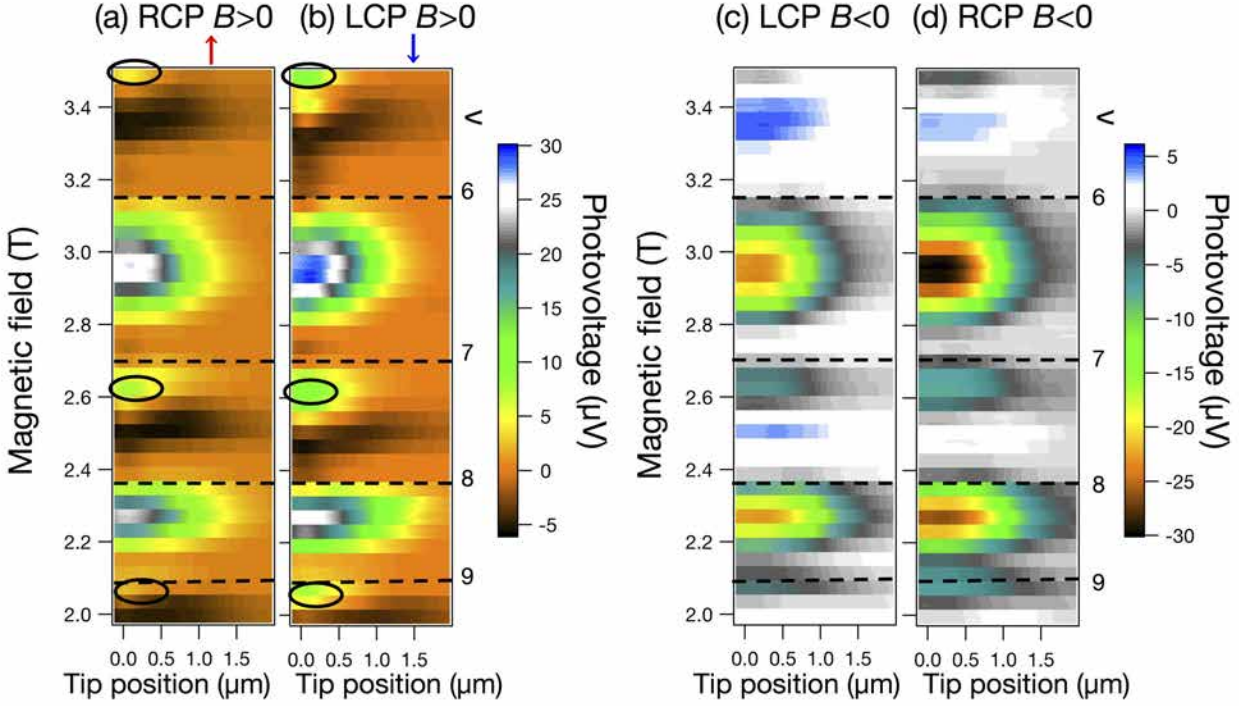


Fig. 5 Color mappings of photovoltage as functions of lateral position and magnetic field for (a) right and (b) left circularly polarized light at $B > 0$, and (c) left and (d) right circularly polarized light at $B < 0$ at the excitation energy of 1.5140 eV. Solid circles in (a) and (b) denote the positions where the photovoltage is larger in LCP than in RCP.

energy of the j th electron state with wavevector k_y and spin s . The red (blue) in Fig. 4 indicates the regions where up- (down-) spin electrons occupy the subband at the Fermi level. The positions of the incompressible strips I and I_s as indicated by the white regions in Fig. 4 move inwards of the sample with increase in the magnetic field. Note here that the positions of I and I_s depend on the curvature of the lateral confinement potential. The positions of I and I_s are closer to the edge of the sample for harder lateral confinement potential $V_4(x)$ as compared to $V_2(x)$.

3.2 Circular polarization dependence of photovoltage mapping

Our circularly polarized NSOM enables us to inject spin polarized electrons locally to the 2DES layer. Figure 5(a) and 5(b) show mappings of photovoltage for right and left circularly polarized light excitation, respectively, as functions of lateral position and magnetic field. Upon illumination of the heterojunction sample, electron-hole pairs are created in the thick GaAs layer. The photoinduced holes move to the rear side whereas the electrons move to the front side of the sample due to the strong vertical electric field in the heterojunction sample. The electrons optically created near the edge of the sample either diffuse to the compressible strips at

the same side of the sample of the laser spot or to the compressible strips at the opposite side of the sample across the bulk region. The diffusion current is balanced by the Hall current, leading to the change of the chemical potential of the edge states [20]. This change of the chemical potential is detected as the Hall photovoltage between the contacts 1 and 2 in Fig. 1.

Periodic photovoltage signals are observed correlated with the bulk electron filling factor ν . The photovoltage is vanishingly small at the integer ν as shown in Fig. 5 at the condition for the quantum Hall effect. The positive photovoltage is observed in Figs. 5(a) and 5(b) at the bulk electron filling factor slightly larger than the integer (ν^+) where the diffusion current across the bulk region is small. This is a consequence of the large width of the innermost I or I_s at ν^+ (w^+) as shown in Fig. 4. By contrast, the negative photovoltage is observed at the bulk electron filling factor slightly smaller than the integer (ν^-), where the diffusion current across the bulk region is large because of the small width of the innermost I or I_s at ν^- (w^-). Inverting the direction of the magnetic field as shown in Figs. 5(c) and 5(d) reverses the sign of the photovoltage.

Clear circular polarization dependence of the photovoltage is observed as shown in Fig. 5. Figures 5(a) and 5(b) show that the photovoltage at 3.5 T ($\nu = 5.4$) is larger in left circular polarization (LCP) where down-

spin electron is optically created than in right circular polarization (RCP) where up-spin electron is created. Similarly, the photovoltage at $\nu = 7.3$ and 9.3 is larger in LCP than in RCP. This circular polarization dependence of the photovoltage is reversed at $B < 0$.

The observed circular polarization dependence of the photovoltage is understood by the type of the innermost incompressible strip, whether it is I_s or I , that separates the bulk and the edge regions [7] as schematically shown in Fig. 6. A spin-split incompressible strip I_s with a width w_a separates the bulk and the edge regions for $2m - 1 < \nu < 2m$, for m integer as shown in Fig. 3(c). Consider here the case where up- or down-spin electrons are optically created in the edge region in Fig. 3(c). The subband energy of the up-spin electron is flat on C_\uparrow adjoining to the innermost incompressible strip I_s at $\nu_L = 5$, whereas the subband energy of the down-spin electron increases with increase in X . Consequently, the diffusion current of the optically created up-spin electrons from the edge across the bulk region is larger than that of the down-spin electrons as schematically shown in Fig. 6(a), resulting in larger photovoltage in LCP (V_+^{LCP}) for creating down-spin electrons than photovoltage in RCP (V_+^{RCP}) as shown in Figs. 5(a) and 5(b). At $2m < \nu < 2m + 1$, a spin-unpolarized incompressible strip I with a width w_b separates the bulk and the edge regions as shown in Fig. 3(d). Because I is formed due to the cyclotron energy $\hbar\omega_c$, this strip is more robust to disorders than I_s which is formed due to the exchange energy-enhanced spin gap as schematically shown in Fig. 6(b). As a consequence the diffusion current of both the up- and down-spin electrons from the edge across the bulk region is small. This explains the small circular polarization dependence of the observed photovoltage in this case.

4 Conclusions

We have demonstrated successful optical spin injection using a circularly polarized near-field optical microscope. Our method should be widely applied to investigate spin dependent phenomena in nanostructured materials.

Acknowledgements We acknowledge the stimulated discussion in the meeting of the Cooperative Research Project of the Research Institute of Electrical Communication, Tohoku University.

References

1. D.W. Pohl, W. Denk, M. Lanz, Appl. Phys. Lett. **44**, 651 (1984)

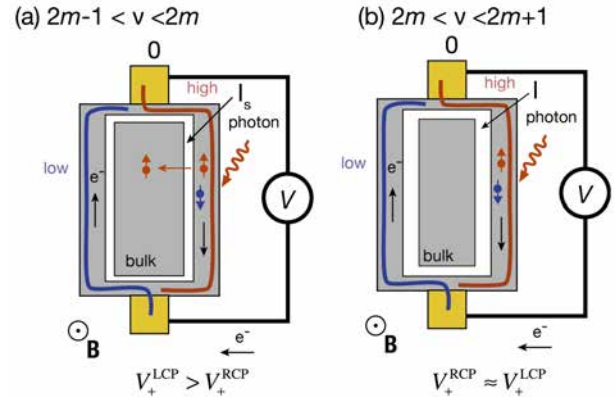


Fig. 6 Schematics of diffusion of electrons near the edge in magnetic field \mathbf{B} for (a) $2m - 1 < \nu < 2m$ for m integer where a spin-split incompressible strip I_s separates the bulk and the edge regions, and (b) $2m < \nu < 2m + 1$ where a spin-unpolarized incompressible strip I separates the bulk and the edge regions.

2. A. Harootunian, E. Betzig, M. Isaacson, A. Lewis, Appl. Phys. Lett. **49**(11), 674 (1986)
3. T. Saiki, K. Nishi, M. Ohtsu, Jpn. J. Appl. Phys. **37**, 1638 (1998)
4. G. Eytan, Y. Yayon, M. Rappaport, H. Shtrikman, I. Bar-Joseph, Phys. Rev. Lett. **81**, 1666 (1998)
5. K. Matsuda, T. Saiki, S. Nomura, M. Mihara, Y. Aoyagi, S. Nair, T. Takagahara, Phys. Rev. Lett. **91**, 177401 (2003)
6. H. Ito, K. Furuya, Y. Shibata, S. Kashiwaya, M. Yamaguchi, T. Akazaki, H. Tamura, Y. Ootuka, S. Nomura, Phys. Rev. Lett. **107**, 256803 (2011)
7. S. Mamyouda, H. Ito, Y. Shibata, S. Kashiwaya, M. Yamaguchi, T. Akazaki, H. Tamura, Y. Ootuka, S. Nomura, Nano Lett. **15**(4), 2417 (2015)
8. T. Saiki, S. Mononobe, M. Ohtsu, N. Saito, J. Kusano, Appl. Phys. Lett. **68**, 2612 (1996)
9. J. Cruz, A. M.V., M. Hernandez, Appl. Opt. **35**(6), 922 (1996)
10. S. Nomura, Y. Aoyagi, Phys. Rev. Lett. **93**, 096803 (2004)
11. G. Giuliani, G. Vignale, *Quantum Theory of the Electron Liquid* (Cambridge Univ. Press, Cambridge, 2005), chap. 7
12. B. Fornberg, D. Sloan, in *Acta Numerica 1994*, eds. A. Iserles (Cambridge University Press, Cambridge, 1994), pp. 203–267
13. I. Vurgaftman, J.R. Meyer, L.R. Ram-Mohan, J. of Appl. Phys. **89**(11), 5815 (2001)
14. D.B. Chklovskii, B.I. Shklovskii, L.I. Glazman, Phys. Rev. B **46**, 4026 (1992)
15. K. Lier, R. Gerhardtts, Phys. Rev. B **50**, 7757 (1994)
16. A. Manolescu, R.R. Gerhardtts, Phys. Rev. B **51**, 1703 (1995)
17. T. Stoof, G. Bauer, Phys. Rev. B **52**, 12143 (1995)
18. S. Ihnatsenka, I.V. Zozoulenko, Phys. Rev. B **73**, 155314 (2006)
19. S. Nomura, H. Tamura, M. Yamaguchi, T. Akazaki, Y. Hirayama, Phys. Rev. B **87**, 085318 (2013)
20. A.A. Shashkin, A.J. Kent, J.R. Owers-Bradley, A.J. Cross, P. Hawker, M. Henini, Phys. Rev. Lett. **79**, 5114 (1997)